Chapter 10

Multiband Planar Antennas for Broadband Wireless Systems

Mohammad Alibakhshi-Kenari,
Mohammad Naser-Moghadasi,
Ramazan Ali Sadeghzadeh, Bal Singh Virdee and
Ernesto Limiti

Additional information is available at the end of the chapter

http://dx.doi.org/10.5772/65802

Abstract

Next generation of wireless mobile systems calls for more compact and multiband antennas. This is because such systems need to be small and can operate over multiple wireless communication standards. The design and development of miniature antennas that function over a wideband are highly challenging. In this chapter, novel antenna designs are presented, which provide a solution to this deficiency. These antennas are based on composite right-/left-handed transmission line (CRLH-TL) metamaterials. Unlike traditional right-handed (RH) transmission materials, metamaterials based on left-handed (LH) transmission lines have unique features of antiparallel group and phase velocities. Pure LH transmission lines cannot be implemented due to the existence of RH parasitic effects that occur naturally in practical LH transmission lines. In this chapter, novel CRLH transmission line structures are presented, which include right-handed parasitic effects.

Keywords: compact antennas, composite right-/left-handed transmission lines, metamaterials, multiband antennas, VHF/UHF antennas

1. Introduction

The design and development of wideband antennas are highly challenging, especially for application in portable wireless communications systems [1]. Due to the limited space assigned

for the antenna in such systems, shrinking the size conventional antennas can lead to degradation in its performance and complicate mechanical assembly. An alternative solution is to employ metamaterial (MTM) technology in the design of antennas. MTM antennas have smaller dimensions because their size is independent of wavelength (λ), which does not compromise its performance [2, 3]. Various implementations of the MTM structures have been reported and demonstrated [4]. In this chapter, a number of identical MTM transmission line (TL) unit cell structures are cascaded together in series to realize a compact antenna with a small footprint. Equivalent model of the MTM-TL unit cell is composed of a series inductor (L_R) and capacitor (C_L), and shunt inductor (L_L) and capacitor (C_R). Components L_L and C_L determine the left-handed (LH) mode propagation properties of the structure, whereas L_R and C_R are parasitic effects resulting from the practical realization of the MTM-TL structure, which determine the right-handed (RH) mode propagation properties. Practical realization of the MTM-TL is commonly referred to as the composite right-/left-handed transmission line (CRLH-TL), which provides a conceptual route for implementing small-sized antennas. The CRLH-TL-based antennas can also be made wideband to support today's multiband wireless communication system needs. The electrical size of a conventional CRLH-TL is strongly related to its physical dimensions, and consequently by reducing its size, we can effectively increase its operational frequency. Physical size of a CRLH-TL is determined by the four aforementioned parameters (C_R, L_R, C_L, and L_L). This implies that if these four parameters are realized in a very compact form, the antenna size will be highly compact and small [5, 6]. A typical realization of CRLH-TL is found in a quasi-lumped transmission line with elementary cells consisting of a series capacitor and a shunt inductor. In practice, the right-handed parasitic effects (C_R and L_R) created by the gap between the microstrip line and ground plane cannot be avoided, which results in unwanted current flow on the radiating patch that can degrade the antenna performance [7–9].

In this chapter, an innovative wideband antenna is designed, fabricated, and tested using a unique metamaterial transmission line unit cell structure. The MTM-TL unit cell is based on distributed implementation of the series capacitor and shunt inductor realized with a slit (L- and F-shaped) and spiral configurations, respectively. The radiating unit cells benefit from miniaturized size, planar structure, low profile, ease of fabrication, light weight, and low cost. In addition, the proposed MTM-TL unit cell provides wideband operation with good radiation properties. The parametric study presented in the chapter shows that the number of unit cells and the slit dimensions can have a dramatic influence on the antenna's performance in terms of operational bandwidth and radiation characteristics. Two antennas are designed for RF applications with maximum size of 14×5 mm^2.

2. Antenna design procedure

2.1. Equivalent circuit model

Equivalent circuit model of the CRLH-TL unit cell, shown in **Figure 1**, consists of C_L, L_L, C_R, and L_R. The circuit model of the purely right-handed transmission line (PRH-TL) is shown

http://dx.doi.org/10.5772/65802

in **Figure 1b**, which is a dual of **Figure 1a** and is a purely left-handed transmission line (PLH-TL), where the series inductor is replaced with a capacitor, and the shunt capacitor is substituted with an inductor. PLH-TL represents an ideal model, which does not exist in practice. Such a structure will have associated parasitic series inductance (L_R) and shunt capacitance (C_R) as well as loss components represented by series conductance (G_L) and shunt conductance (G_R). A more realistic equivalent circuit model of PLH-TL, shown in **Figure 1c**, is a combination of left-handed and right-handed transmission line, which is referred to as composite right-/left-handed transmission. At low frequency, C_L and L_L are dominant, and hence the transmission line exhibits left-handed characteristics; however, at high frequency, L_R and C_R are dominant, which makes the transmission line exhibit right-handed characteristics.

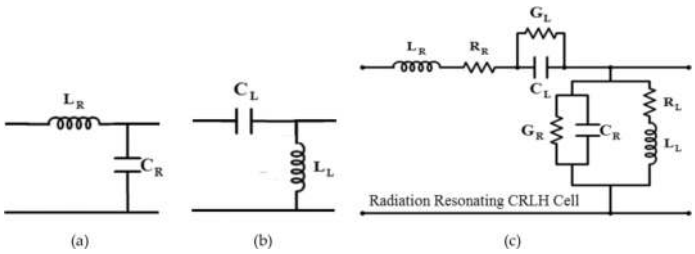

Figure 1. Equivalent circuit model of: (a) purely right-handed transmission line, (b) purely left-handed transmission line, and (c) CRLH-TL with loss.

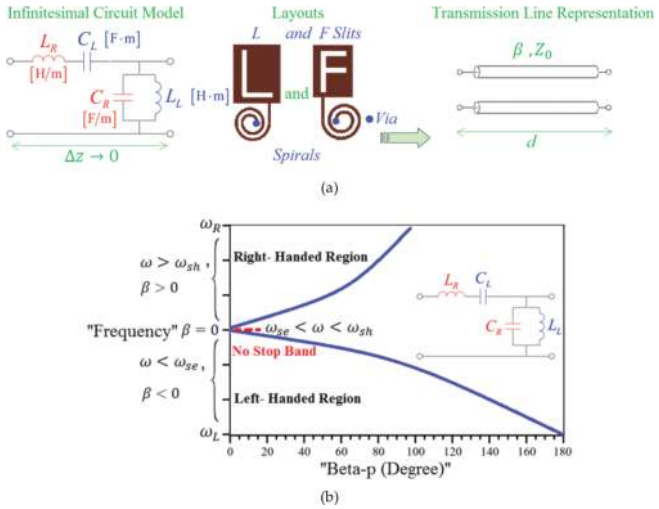

Figure 2. (a) Simplified loss-less equivalent circuit model of the CRLH-TL unit cells and its implementation with L- and F-shaped slit, and (b) dispersion diagram of the CRLH-TL unit cells.

The simplified circuit model and layouts of the proposed CRLH unit cell structures are shown in **Figure 2a**, where capacitance (C_L) is implemented with the either L-shaped or F-shaped slits in the microstrip patch, and inductance (L_L) is implemented with a spiral that is ground plane through via-hole. Capacitance (C_R) is associated with the gap between the microstrip section and the ground plane, and inductance (L_R) is associated with the microstrip patch. The unit cells are designed using conventional microwave integrated technology. The unit cell can be easily implemented and is a low-profile design. As shown below, wideband antennas can be designed by simply cascading together in series an appropriate number of unit cells for operation across VHF and UHF bands.

The CRLH-TL unit cell topologies in **Figure 2a** has a propagation constant (γ) given by:

$$\gamma = \alpha + j\beta = \sqrt{ZY} \tag{1}$$

where

$$\beta(\omega) = s(\omega)\sqrt{\omega^2 L_R C_R + \frac{1}{\omega^2 L_L C_L} - \left(\frac{L_R}{L_L} + \frac{C_R}{C_L}\right)} \tag{2}$$

$$s(\omega) = \begin{cases} -1 if \omega < \omega_{se} = min\left(\frac{1}{\sqrt{L_R C_L}}, \frac{1}{\sqrt{L_L C_R}}\right) \\ 0 if \omega_{se} < \omega < \omega_{sh} \\ +1 if \omega > \omega_{sh} = max\left(\frac{1}{\sqrt{L_R C_L}}, \frac{1}{\sqrt{L_L C_R}}\right) \end{cases} \tag{3}$$

and

$$Z(\omega) = j(\omega L_R - 1/\omega C_L) \tag{4}$$

$$Y(\omega) = j(\omega C_R - 1/\omega L_L) \tag{5}$$

Parameters $\beta(\omega)$, $s(\omega)$, $Z(\omega)$, and $Y(\omega)$ are a function of frequency and related to dispersion, sign function, impedance, and admittance of the antenna structure, respectively. The series and shunt resonance frequencies, respectively, are:

$$\omega_{se} = \frac{1}{\sqrt{L_R C_L}} \tag{6}$$

$$\omega_{sh} = \frac{1}{\sqrt{L_L C_R}} \tag{7}$$

The phase and group velocities, respectively, are defined by:

$$v_p = \frac{\omega}{\beta} = \omega^2 \sqrt{L_L C_L} \tag{8}$$

$$v_g = \left(\frac{\partial \beta}{\partial \omega}\right)^{-1} = \omega^2 \sqrt{L_L C_L} \tag{9}$$

The dispersion diagram of the proposed CRLH unit cells is shown in **Figure 2b**. Bandwidth of CRLH-TL unit cells is defined between the high-pass (left-handed) cutoff frequency (ω_L) and the low-pass (right-handed) cutoff frequency (ω_R). The cutoff frequencies ω_L and ω_R are given by:

$$\omega_L = \frac{1}{\sqrt{L_L C_L}} \tag{10}$$

$$\omega_R = \frac{1}{\sqrt{L_R C_R}} \tag{11}$$

The CRLH-TL unit cells were designed and constructed on Rogers RT/duroid® RO4003 substrate with dielectric constant of $\varepsilon_r = 3.38$, thicknesses of $h = 0.8$ and 1.6 mm, and tan $\delta = 0.0022$. The L- and F-shaped unit cells occupied a space of $2.3 \times 4.9 \times 0.8$ mm^3 and $2.06 \times 4.4 \times 1.6$ mm^3, respectively. Microstrip feed line is used to excite the unit cells from the right-hand side of the structure, which is terminated on the left-hand side with a 50 Ω load (i.e., SMD1206), which is 4.2 mm long. The antenna design was modeled and analyzed with a 3-D full-wave electromagnetic field simulator from Ansys called High Frequency Structure Simulator (HFSS™) [10]. The optimized antennas were fabricated and tested, and the results are presented below.

2.2. Metamaterial antenna with L-shaped slits

The CRLH-TL unit cell consists of a rectangular radiation patch on which is engraved an L-shaped slit, and the patch is inductively grounded with a high-impedance spiral stub. The L-shaped slit acts like a LH capacitance (C_L), and the inductive spiral whose end is connected to

the ground plane metallic via-holes acts like a LH inductance (L_L). In reality, the LH reactive components are accompanied with RH parasitic effects represented by series inductance (L_R) and shunt capacitance (C_R) resulting from current flow in the microstrip metallization and voltage gradient created between the metal pattern of the microstrip and the ground plane. Thus, the unit cell is more accurately represented by a composite right-/left-handed model with the inclusion of resistive and conductance loss components represented by R_R, R_L and G_R, G_L, respectively, which account for the ohmic and dielectric loss associated with the unit cell. Four CRLH-TL unit cells were cascaded together in series, as shown in **Figure 3**, to implement an antenna design for application in VHF band (30–300 MHz) and UHF band (300 MHz–3 GHz). The antenna structure was optimized using HFSS™.

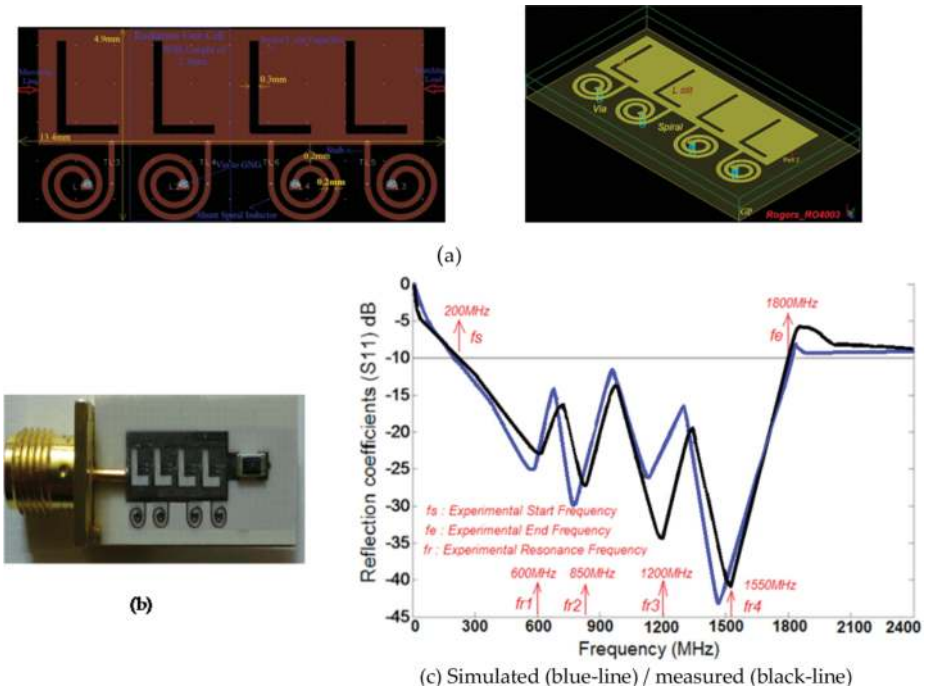

Figure 3. CRLH-TL antenna configuration with four L-shaped slits on the RT/duroid® RO4003 substrate with thickness of 0.8 mm, (a) distributed implementation (top isometric view), (b) fabricated prototype, and (c) reflection coefficient response of the antenna.

Besides the small dimensions, the bandwidth and good radiation properties are other main performance criteria in the antenna systems. With the proposed antenna design, the bandwidth can be increased by simply introducing more unit cells. Hence, there is a tradeoff between size of the antenna, bandwidth and radiation properties. Each cell occupies an area of 2.3 × 4.9 mm^2. Dimensions of the L-shaped slit antenna are 13.4 × 4.9 × 0.8 mm^3 or $0.0089\lambda_o \times 0.0032\lambda_o \times 0.00053\lambda_o$, where λ_o is free-space wavelength at 200 MHz.

http://dx.doi.org/10.5772/65802

For the L-shaped antenna, the simulated bandwidth is 1625 MHz (195 MHz–1.82 GHz) using HFSS™, and the measured bandwidth is 1600 MHz (200 MHz–1.8 GHz) for VSWR ≤ 2, which corresponds to a fractional bandwidth of 160%. The reflection coefficient response of the antenna, shown in **Figure 3**, clearly indicates its resonates at four distinct frequencies of 600, 850, 1200, and 1550 MHz. The measured gain and efficiency of the antenna are 1.2 dBi and 34% at 600 MHz, 1.7 dBi and 45% at 850 MHz, 2.1 dBi and 62% at 1200 MHz, and 3.4 dBi and 88% at 1550 MHz. The measured 2D and simulated 3D radiation patterns of the antenna are shown in **Figure 4** at the various resonance frequencies. The measured antenna gain and efficiency response are shown in **Figure 4c**.

The simulated and measured radiation patterns of the antenna at various frequencies in the two principle planes, the *x*-*z* and *x*-*y* planes, are shown in **Figure 4**. The antenna has approximately omnidirectional radiation patterns in the *x*-*z* plane. The *x*-*y* plane patterns show two nulls in the *y*-direction, which is similar to a typical monopole antenna.

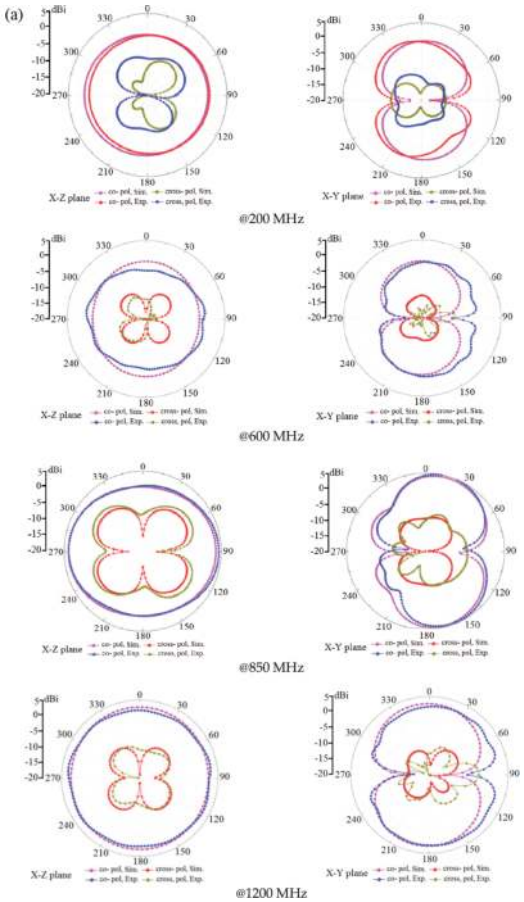

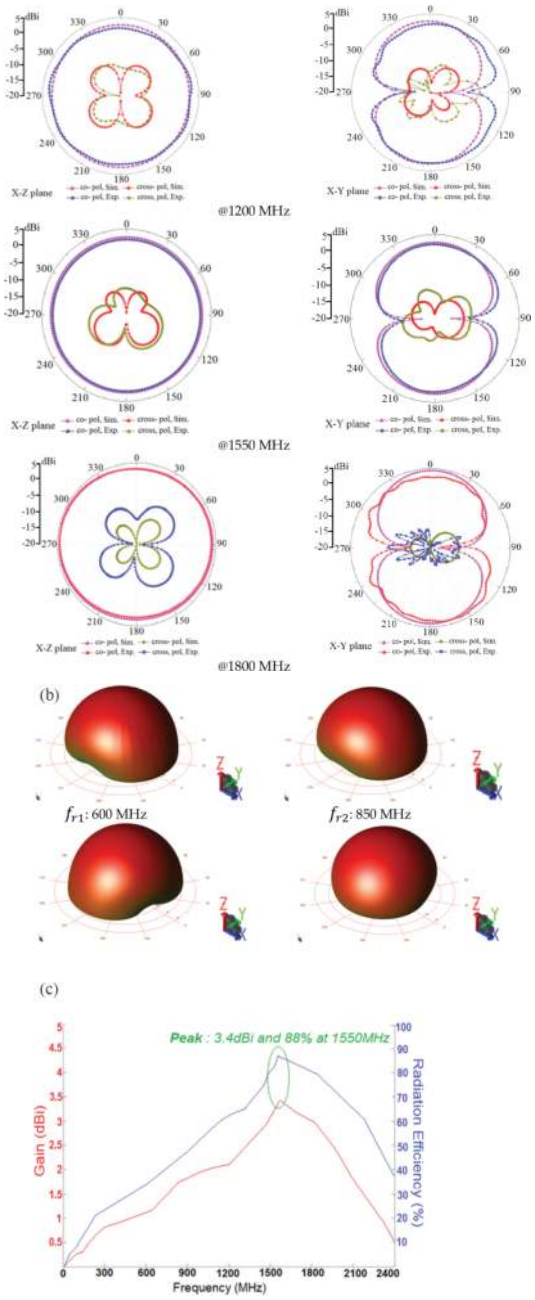

Figure 4. Radiation patterns of the L-shaped antenna, (a) measured 2D patterns, (b) simulated 3D patterns, and (c) measured gain and efficiency response.

http://dx.doi.org/10.5772/65802

2.3. Metamaterial antenna with F-shaped slits

In this section, the main goal is to design and implement an antenna with better performance than the above L-shaped antenna. This was achieved by modifying the L-shaped antenna by changing the slits to F-shaped. The equivalent circuit model of the unit cell is shown in **Figures 1** and **2**. In this case, the optimized antenna employed five CRLH-TL unit cells, as shown in **Figure 5a**. Each unit cell occupied an area of $2.06 \times 4.40\ mm^2$ ($0.00075\lambda_o \times 0.0016\lambda_o$) at 110 MHz. Dimensions of the antenna are $14.5 \times 4.4 \times 1.6\ mm^3$ or $0.0053\lambda_o \times 0.0016\lambda_o \times 0.00058\lambda_o$, where λ_o is free-space wavelength at 110 MHz. Each unit cell occupied an area of $2.06 \times 4.40\ mm^2$ ($0.00075\lambda_o \times 0.0016\lambda_o$) at 110 MHz.

The antenna was fabricated on RT/duroid® RO4003 substrate with thickness of 1.6 mm. The reflection coefficient response of the antenna in **Figure 5b** shows that the antenna has a measured impedance bandwidth of 1.99 GHz (110 MHz–2.10 GHz) for VSWR ≤ 2, which corresponds to a fractional bandwidth of 180.1%. The antenna resonates at 450, 725, 1150, 1670, and 1900 MHz.

The measured gain and efficiency of the F-shaped antenna, shown in **Figure 5c**, are 1.0 dBi and 31% at 450 MHz, 1.8 dBi and 47% at 725 MHz, 2.5 dBi and 70% at 1150 MHz, 3.8 dBi and 89% at 1670 MHz, and 4.5 dBi and 95% at 1900 MHz.

(a) Fabricated prototype

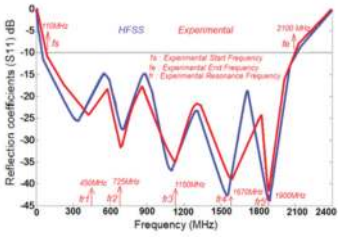

(b) Reflection coefficient response.
Simulated (blue-line) and measured (red-line)

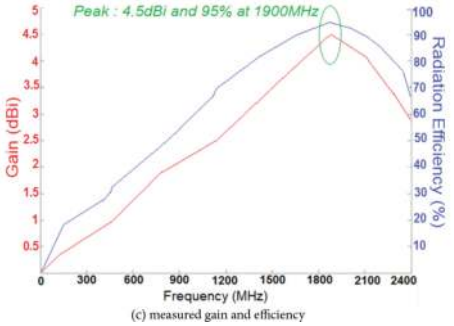

(c) measured gain and efficiency

Figure 5. Five CRLH-TL unit cell antenna configuration with F-shaped slit designed on RT/duroid® RO4003 with thickness 1.6 mm, (a) fabricated photograph and (b) reflection coefficient as function of frequency (c) measured gain and efficiency versus frequency.

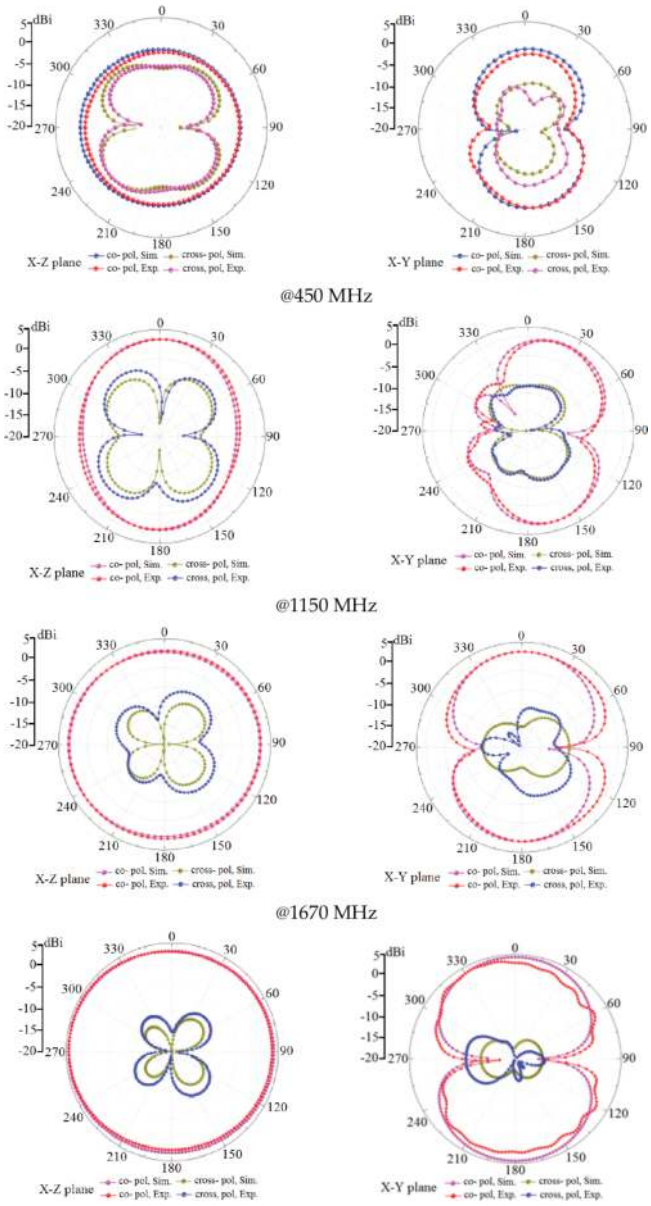

Figure 6. 2D radiation patterns of the F-shape slit CRLH-TL antenna.

The simulated and measured radiation patterns of the antenna in the *x*-*z* and *x*-*y* planes at various spot frequencies are shown in **Figure 6**. It is evident that the measured radiation patterns agree well with the simulation results. The results show that the radiation is omni-

http://dx.doi.org/10.5772/65802

directional in the *x*-*z* plane over a wideband frequency range. In the *x*-*y* plane, the radiation is null in the positive and negative *y* directions, which is typical for monopole antennas.

3. Analysis on antenna design parameters

To achieve the desired antenna performance, the number of unit cells (n), number of spiral turns (N_{SP}), spiral width (W_{SP}), and distances between spirals (S_{SP}) need to be optimized, which was done using Ansys HFSS™ EM Simulator. **Figures 7–12** show the effect of these parameters on the reflection coefficient response of the antenna. **Figure 7** shows that the bandwidth is improved from 43.47% for one unit cell to 180.1% for five unit cells. The increase in unit cells has also increased the number of resonance spikes.

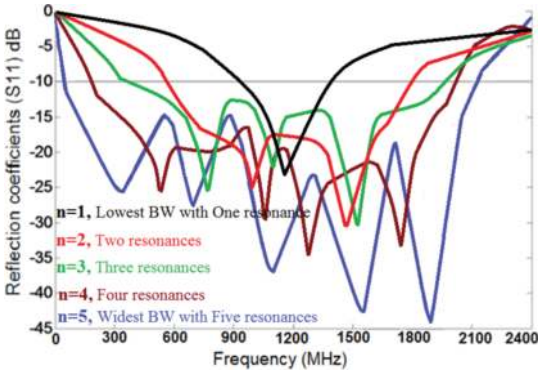

Figure 7. Reflection coefficient response of the proposed antenna as a function of number of unit cells.

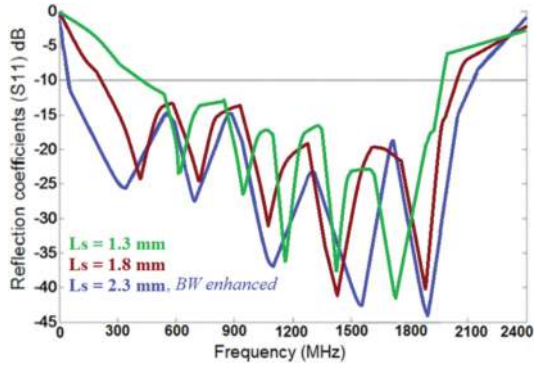

Figure 8. Reflection coefficient response of the antenna as a function of the vertical slit length. The slit width was kept fixed at 0.3 mm.

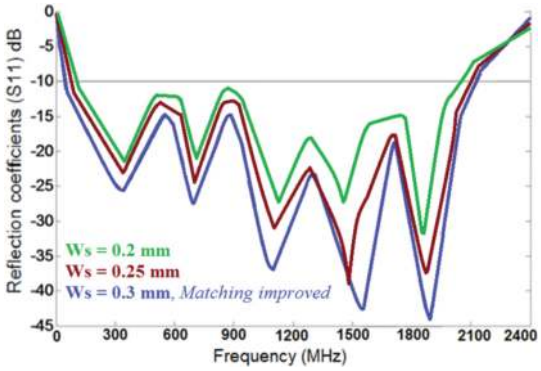

Figure 9. Reflection coefficient response of the antenna as a function of the slit width.

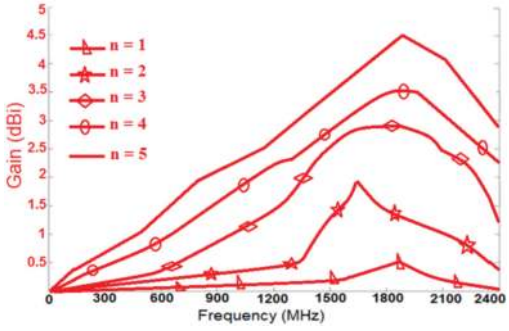

Figure 10. Antenna gain versus frequency with variation in number of unit cells ($n = 1$–4 for simulation and $n = 5$ is measured). Length was fixed at 2.3 mm.

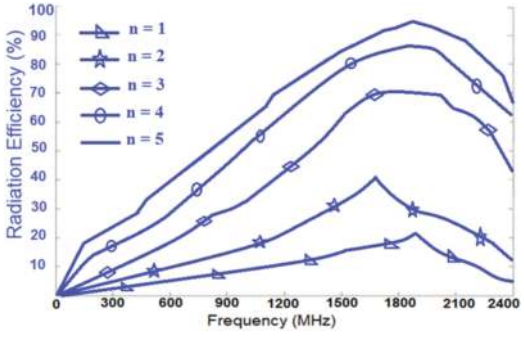

Figure 11. Antenna efficiency versus frequency with variation in number of unit cells ($n = 1$–4 for simulation and $n = 5$ is measured).

http://dx.doi.org/10.5772/65802

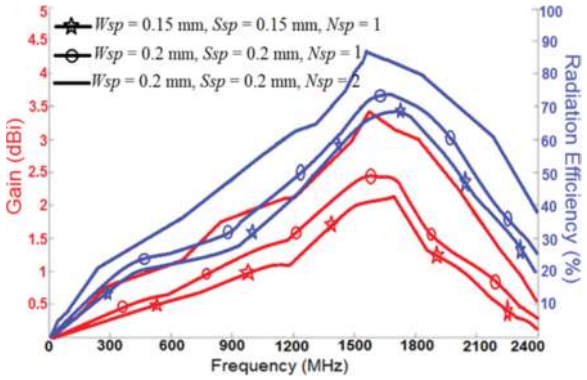

Figure 12. Gain and efficiency response as a function of spiral width (W_{SP}), distances between spirals (S_{SP}) and number of spiral turns (N_{SP}).

References (UC: unit cells)	Dimensions (ES: electrical size, PHS: physical size)	Fractional bandwidth	Gain (Max)	Eff. (Max)
[11] b-shaped antenna with 4×UC	ES: $0.047\lambda_o \times 0.021\lambda_o \times 0.002\lambda_o$ at 1 GHz, PHS: 14.2 × 6.32 × 0.8 mm^3	104.76% (1–3.2 GHz)	2.3 dBi	62%
[11] b-shaped antenna with 6×UC	ES: $0.051\lambda_o \times 0.016\lambda_o \times 0.002\lambda_o$ at 0.8 GHz, PHS: 19.2 × 6.32 × 0.8 mm^3	123.8% (0.8–3.4 GHz)	2.8 dBi	70%
[12] J-shaped antenna with 8×UC	ES: $0.564\lambda_o \times 0.175\lambda_o \times 0.02\lambda_o$ at 7.5 GHz, PHS: 22.6 × 7 × 0.8 mm^3	84.23% (7.25–17.8 GHz)	2.3 dBi	48%
[12] I-shaped antenna with 7×UC	ES: $0.556\lambda_o \times 0.179\lambda_o \times 0.041\lambda_o$ at 7.7 GHz, PHS: 21.7 × 7 × 1.6 mm^3	87.16% (7.8–19.85 GHz)	3.4 dBi	68.1%
[12] J-shaped antenna with 6×UC	ES: $0.45\lambda_o \times 0.175\lambda_o \times 0.02\lambda_o$ at 7.5 GHz, PHS: 18 × 7 × 0.8 mm^3	74.4% (7.5–16.8 GHz)	2.1 dBi	44.3%
[12] I-shaped antenna with 5×UC	ES: $0.428\lambda_o \times 0.179\lambda_o \times 0.041\lambda_o$ at 7.7 GHz, PHS: 16.7 × 7 × 1.6 mm^3	82.88% (7.7–18.6 GHz)	3.1 dBi	58.6%
[13]	ES: $0.134\lambda_o \times 0.035\lambda_o \times 0.002\lambda_o$ at 0.67 MHz, PHS: 60 × 16 × 1 mm^3	116.7% (0.67–2.55 GHz)	4.7 dBi	62.9%
[14]	ES: $0.108\lambda_o \times 0.108\lambda_o \times 0.009\lambda_o$ at 1.8 GHz,PHS: 18 × 18 × 1.6 mm^3	26.5% (1.8–2.35 GHz)	3.7 dBi	20%
[15]	ES: $0.164\times\lambda_o \times 0.013\ \lambda_o \times 0.013\lambda_o$ att 0.8 MHz, PHS: 60 × 5 × 5 mm^3	103.03% (0.8–2.5 GHz)	0.4 dBi	53.6%
[16]	ES: $0.06\lambda_o \times 0.06\lambda_o \times 0.021$ aλ_o at 1 GHz, PHS: 18.2 × 18.2 × 6.5 mm^3	66.66% (1–2 GHz)	0.6 dBi	26%
Proposed F-shaped slit antenna 5×UC	ES: $0.0053\lambda_o \times 0.0016\lambda_o \times 0.00058\lambda_o$ at 0.11 MHz, PHS: 14.5 × 4.4 × 1.6 mm^3	180.1% (0.11–2.1 GHz)	4.5 dBi	95%

Table 1. Comparison of the antenna characteristics.

Figure 8 indicates that the larger the vertical length of the slit, the larger the bandwidth (for S_{11} < -10 dB). Increase in slit length from 1.3 to 2.3 mm increases the bandwidth by 36.5%.

Figure 9 shows that the increase in the width from 0.2 to 0.3 mm increases the bandwidth by 9.3%. The gain and the radiation efficiency of the antenna are greatly affected by the number of unit cells. The peak gain and radiation efficiency increase substantially with the number of unit cells as shown in **Figures 10** and **11**. The measured peak gain and peak radiation efficiency are 4.5 dBi and 94.8% for five unit cells at 1890 MHz. **Figure 12** shows that the spiral width, their separation and number of turns also affect the antenna's gain and radiation efficiency.

Features of the proposed two antennas are compared with other similar antennas in **Table 1**.

Acknowledgements

The authors would like to give special thanks to faculty of Microelectronics for financial support.

Author details

Mohammad Alibakhshi-Kenari[1*], Mohammad Naser-Moghadasi[2],
Ramazan Ali Sadeghzadeh[3], Bal Singh Virdee[4] and Ernesto Limiti[1]

*Address all correspondence to: naeem.alibakhshi@yahoo.com

1 Dipartimento di Ingegneria Elettronica, Università degli Studi di Roma Tor Vergata, Via del Politecnico, Roma, Italy

2 Faculty of Engineering, Science and Research Branch, Islamic Azad University, Tehran, Iran

3 Faculty of Electrical Engineering, K. N. Toosi University of Technology, Tehran, Iran

4 London Metropolitan University, Center for Communications Technology, London, UK

References

[1] J. Anguera, A. Andújar, M.C. Huynh, C. Orlenius, C. Picher, and C. Puente, "Advances in antenna technology for wireless handheld devices," *International Journal of Antennas and Propagation*, Volume 2013 (2013), Article ID 838364, 25 pages http://dx.doi.org/10.1155/2013/838364

[2] C. Caloz and T. Itoh. *Electromagnetic Metamaterials: Transmission Line Theory and Microwave Applications*, 2005, Wiley. ISBN: 978-0-471-66985-2 376 pages December 2005, Wiley-IEEE Press

[3] N. Engheta and R.W. Ziolkowski, *Metamaterials: Physics and Engineering Explorations*, 2006, Wiley. ISBN: ISBN: 978-0-471-66985-2 376 pages December 2005, Wiley-IEEE Press

[4] R.A. Shelby, D.R. Smith, and S. Schultz, "Experimental verification of a negative index of refraction," *Science*, 2001; 292(5514): 77–79. doi:10.1126/science.1058847

[5] C.J. Lee, M. Achour, and A. Gummalla, "Compact metamaterial high isolation MIMO antenna subsystem," *Asia Pacific Microwave Conference*, 2008: 1–4. doi:10.1109/APMC.2008.4957946

[6] C.J. Lee, K.M.H. Leong, T. Itoh, "Broadband small antenna for portable wireless application," *International Workshop on Antenna Technology: Small Antennas and Novel Metamaterials*," *iWAT* 2008: 10–l3.

[7] M. Alibakhshi-Kenari, M. Movahhedi and H. Naderian, "A new miniature ultra wide band planar microstrip antenna based on the metamaterial transmission line," *IEEE Asia-Pacific Conference on Applied Electromagnetics*, 2012: 293–297. doi:10.1109/APACE.2012.6457679

[8] M. Alibakhshi-Kenari, "A new compact UWB traveling-wave antenna based on CRLH-TLs for embedded electronic systems," *International Journal of Microwave and Wireless Technologies*, 2014: 1–4. doi:10.1017/S1759078714001020

[9] J.D. Jackson, *Classical Electromagnetics*, Wiley, New York, 3rd ed., 1999.

[10] Ansoft HFSS, www.ansoft.com/products/hf/hfss.

[11] M. Alibakhshi-Kenari, "Printed planar patch antennas based on metamaterial," *International Journal of Electronics Letters*, Volume 2, Issue 1, Jan. 2014, pp 37–42

[12] M. Alibakhshi-Kenari, "Introducing the new wide band small plate antennas with engraved voids to form new geometries based on CRLH MTM-TLs for wireless applications," *International Journal of Microwave and Wireless Technologies*, 2014; 6(06): 629–637. doi:10.1017/S1759078714000099

[13] J. Luo, S. Gong, P. Duan, C. Mou, and M. Long, "Small-size wideband monopole antenna with CRLH-TL for LTE mobile phone," *Progress in Electromagnetics Research C*, 2014; 50: 171–179.

[14] M.A. Abdalla, A.A. Awad, K.M. Hassan, "Wide band high selective compact metamaterial antenna for 2 GHz wireless applications," *Antennas and Propagation Conference (LAPC)*, 2014: 350–354. doi:10.1109/LAPC.2014.6996395

[15] Y. Li, Z. Zhang, J. Zheng and Z. Feng, "Compact heptaband reconfigurable loop antenna for mobile handset," *IEEE Antennas and Wireless Propagation Letters*, 2011; 10: 1162–1165. doi:10.1109/LAWP.2011.2171311

[16] Lee, C.J., Leong, K.M.K.H., Itoh, T.: 'Composite right/left-handed transmission line based compact resonant antennas for RF module integration', IEEE Trans. Antennas Propag., 2006, 54, (8), pp. 2283–2291.